Structural studies of viperin, an antiviral radical SAM enzyme

Michael K. Fenwick[§,1], Yue Li[//,1], Peter Cresswell[//*], Yorgo Modis[$*], Steven E. Ealick[§*]

[§]*Department of Chemistry and Chemical Biology, Cornell University, Ithaca, NY 14853,USA* [//] *Department of Immunobiology, Yale University School of Medicine, New Haven, CT, 06520, USA and* [$]*Department of Medicine, University of Cambridge, MRC Laboratory of Molecular Biology, Francis Crick Avenue, Cambridge CB2 0QH, UK*

This work was supported by a Wellcome Trust Senior Research Fellowship to Y.M. (101908/Z/13/Z), by National Institutes of Health grants DK067081 to S.E.E, and GM102869 to Y.M., and by the Howard Hughes Medical Institute (P.C.). The work is based upon research conducted at the Advanced Photon Source on the Northeastern Collaborative Access Team beamlines, which are supported by award GM103403 from the NIH. Use of the Advanced Photon Source is supported by the U.S. Department of Energy, Office of Basic Energy Sciences, under Contract No. DE-AC02-06CH11357.

[‡] The coordinates of viperin with bound SAH and with bound 5′-dAdo and L-Met have been deposited in the Protein Data Bank under accession code XXXX and YYYY, respectively.

[1]These authors contributed equally this work.

[*]To whom correspondence should be addressed:

E-mail: peter.cresswell@yale.edu, ymodis@mrc-lmb.cam.ac.uk, see3@cornell.edu

Classification: Immunology and Inflammation; Biophysics and Computational Biology

Keywords: Antiviral response, interferon, radical, *S*-adenosylmethionine

Short Title: Crystal structure of viperin

Abbreviations

SAM, *S*-adenosylmethionine; SAH, *S*-adenosylhomocysteine; DTT, dithiothreitol; RMSD, root mean square deviation; PEG, polyethylene glycol

Abstract

Viperin is an interferon-inducible radical *S*-adenosylmethionine (SAM) enzyme that inhibits viral replication. We determined crystal structures of an anaerobically prepared fragment of mouse viperin (residues 45-362) complexed with *S*-adenosylhomocysteine (SAH) or 5′-deoxyadenosine (5′-dAdo) and L-Met. Viperin contains a partial $(\beta\alpha)_6$-barrel fold with a disordered N-terminal extension (residues 45-74) and a partially ordered C-terminal extension (residues 285-362) that bridges the partial barrel to form an overall closed barrel structure. Cys84, Cys88, and Cys91 located after the first β-strand bind a [4Fe-4S] cluster. The active site architecture of viperin with bound SAH (a SAM analogue) or 5′-dAdo and L-Met (SAM cleavage products) is consistent with the canonical mechanism of 5′-deoxyadenosyl radical generation. The viperin structure together with sequence alignments suggest that vertebrate viperins are highly conserved and that fungi contain a viperin-like ortholog. Many bacteria and archaebacteria also express viperin-like enzymes with conserved active site residues. Structural alignments show that viperin is similar to several other radical SAM enzymes including the molybdenum cofactor biosynthetic enzyme MoaA and RlmN, which methylates specific nucleotides in ribosomal and transfer RNA. The viperin putative active site contains several conserved positively charged residues and a portion of the active site shows structural similarity to the guanosine triphosphate binding site of MoaA, suggesting that the viperin substrate may be a nucleoside triphosphate of some type.

Significance

We report the first structures of viperin, an antiviral radical SAM enzyme. The overall structure shows a canonical radical SAM enzyme fold that harbors a [4Fe-4S] cluster. Structures with a bound SAM analogue or SAM cleavage products are consistent with a conventional mechanism of radical formation. Sequence alignments guided by the putative active site residues of viperin reveal viperin-like enzymes in species from all kingdoms of life. Structural alignments show similarity between viperin and the molybdenum cofactor biosynthetic enzyme MoaA and show that the active site architecture of viperin is consistent with a nucleoside triphosphate substrate.

/body

Introduction

Viruses exploit the metabolic machinery of host cells in order to replicate and spread to other cells. While cytotoxic T-cells and antibody-producing B-cells can ultimately be produced in an adaptive response to the virus, innate immune mechanisms are used to rapidly respond to infection. Upon infection, cells can sense the presence of virus via pattern recognition receptors (1, 2) and produce interferons that limit the spread of infection to other cells (3). Interferons induce the expression of hundreds of interferon-stimulated genes (ISGs), many of which are involved in various antiviral processes, including antigen presentation, apoptosis, and inhibition of viral replication (4-7).

Viperin, the product of *rsad-2*, was first identified as a protein induced by exposure of human macrophages to interferon-γ, and by infection of primary human fibroblasts with human cytomegalovirus (8, 9). Early studies showed that viperin is induced in various cell types by interferon-α and -β, associates with the cytosolic face of the endoplasmic reticulum (ER), and inhibits human cytomegalovirus replication when pre-expressed in human fibroblasts (8). Since then, viperin has been shown to be induced by several factors, including lipopolysaccharide (10-12), and to inhibit a broad range of viruses, including human immunodeficiency virus-1 (HIV-1) (13), West Nile virus (14), hepatitis C virus (15, 16), dengue virus type-2 (17), influenza A virus (18), and tick borne encephalitis virus (19). Gene-profiling microarray studies have shown that the viperin gene is one of the most highly inducible ISGs upon infection with a wide range of RNA viruses (20).

The amino acid sequence of viperin contains a CxxxCxxC motif, characteristic of the radical *S*-adenosylmethionine (SAM) superfamily (8, 21), which is usually characterized structurally by a $(\beta\alpha)_8$-barrel or partial $(\beta\alpha)_6$-barrel fold (22). Radical SAM enzymes use a

[4Fe-4S] cluster to reductively cleave SAM to generate a radical, which is typically transferred to a substrate via hydrogen atom abstraction (23-31). The cysteine residues within the CxxxCxxC motif ligate three of the iron atoms of the [4Fe-4S] cluster. Recombinant viperin has been shown to bind a [4Fe-4S] cluster and reductively cleave SAM (32), and mutation of the cysteine residues of the CxxxCxxC motif to alanine significantly diminishes the antiviral effects of viperin in HIV-1-infected (13) or hepatitis C virus-infected cells (16). While viperin appears to be a radical SAM enzyme, neither the reaction it catalyzes nor its substrate have been identified.

In the present study, we prepared and crystallized *Mus musculus* viperin under anaerobic conditions and determined crystal structures of viperin complexes with the SAM analogue *S*-adenosylhomocysteine (SAH) or the SAM cleavage products 5′-deoxyadenosine (5′-dAdo) and L-Met. The structures reveal the active site architecture and identify key active site residues. The active site architecture together with multiple sequence alignments shows that vertebrate viperins are highly conserved, and that fungi, bacteria, and archaebacteria express viperin-like enzymes. Structural alignments show similarity between viperin and the molybdenum cofactor biosynthetic enzyme MoaA and the RNA methyltransferease RlmN. The similarity extends to portions of the viperin and MoaA active sites.

Results and Discussion

Crystallization and Structure Determination. We crystallized an N-terminally truncated (Δ44 or Δ46) form of *M. musculus* viperin containing a [4Fe-4S] cluster under anaerobic conditions. The truncation removes an amphipathic α-helix near the N-terminus responsible for ER and lipid droplet association and results in a water-soluble derivative (33, 34).

Crystal structures were determined for viperin bound to SAH at 2.0 Å resolution and 5′-dAdo and L-Met at 1.7 Å resolution (Tables S1 and S2). The crystals belong to space group $P2_12_12_1$ and the asymmetric unit contains two molecules of viperin, each with ligands bound. Electron density maps show clear electron density for the ligands and high occupancies for the four iron atoms of the [4Fe-4S] cluster (Fig. S1).

Overall Structure. Viperin is a globular protein containing a partial $(\beta\alpha)_6$-barrel fold (residues 75-284) observed in other radical SAM enzymes (22). Residues 45-73 at the N-terminus and residues 337-362 at the C-terminus are disordered. The overall fold of viperin is illustrated in Fig. 1A and B. The partial $(\beta\alpha)_6$-barrel is augmented by a β-strand (β_7), a β-hairpin (β_8 and β_9), and three α-helices (α_7, α_8, and α_9) from the C-terminal extension. β_7 forms hydrogen bonds with β_6, β_8 forms hydrogen bonds with β_1, and β_7 and β_8 are connected by a segment containing a short α-helix (α_7). The C-terminal extension folds over the open portion of the partial $(\beta\alpha)_6$-barrel resulting in an overall closed barrel structure similar to a $(\beta\alpha)_8$-barrel. β_9 and α_8 are connected by a 12-residue loop in which $G_{316}GRKD_{320}$ of the loop are disordered. The final 26 residues of the protein, which follow α_9, are disordered. C-terminal truncations have been shown to reduce the effectiveness of viperin against HIV-1 (13), hepatitis C virus (16), and dengue virus type-2 (17) suggesting that the C-terminus may be required for interactions with a binding partner. Indeed, viperin interaction with the cytosolic Fe/S cluster assembly factor CIAO1 depends on the conserved viperin C-terminal tryptophan residue, suggesting that viperin lacking the C-terminal region is likely to be enzymatically inactive (19). Residues 50-74 of the N-terminal extension are predicted to be disordered based on analysis of the amino acid sequence (Fig. S2) (35). This region may act as a flexible linker that aids membrane localization (33, 34) and enhances molecular mobility after localization.

Canonical Radical SAM Enzyme Structure. The viperin β-barrel fold contains the radical SAM enzyme hallmark CxxxCxxC motif (C_{84}NYKC_{88}GFC_{91}) located after strand β_1. The three cysteine side chains of the motif ligate three irons of a [4Fe-4S] cluster and position the differentiated iron (not ligated by a cysteine side chain) near the center of the putative active site. The interactions made between viperin and SAH, 5′-dAdo, and L-Met are consistent with known radical SAM enzyme structures (Fig. 1C and D). SAH and L-Met anchor to the differentiated iron of the [4Fe-4S] cluster via their α-amino and α-carboxylate groups (28, 36). The α-amino group also forms hydrogen bonds with a conserved GGE motif ($G_{125}G_{126}E_{127}$) (21, 22), and the α-carboxylate group also forms hydrogen bonds with an arginine and serine side chain (Arg194 and Ser180) (37). The ribose moiety of SAH and 5′-dAdo forms hydrogen bonds with the Arg194 and Ser180 side chains and its O3′-hydroxyl group is within hydrogen bonding distance of the side chain of Asn222. The adenine moiety of SAH and 5′-dAdo is interposed between hydrophobic residues in or near the cluster-binding loop (Phe90 and Phe92), in β_5 (Val224), and near the end of β_6 (Phe249 and Leu252). The adenine moiety also forms hydrogen bonds with polar sites near the cluster-binding loop and near the end of β_6 (Fig. 1C and D).

The binding modes of SAH and L-Met with the [4Fe-4S] cluster are consistent with the ability of viperin to reductively cleave the C5′-S bond of SAM (Fig. S3) (32) and are similar to the binding modes observed in high resolution crystal structures of other radical SAM enzymes (Fig. S4) (28, 38-43). In the proposed mechanism of radical generation, a reduced [4Fe-4S] cluster delivers an electron to the sulfonium ion of SAM to homolytically cleave the C5′-S bond (44). This requires a nearly linear arrangement of C5′, S, and Fe (45); typical C5′-S distances are 3.2-3.7 Å and C5′-S-Fe angles are ~150° (Fig. 1C, Fig. S3A, and Fig. S4A). After cleavage of the C5′-S bond, the sulfur atom of L-Met is expected to coordinate to the differentiated iron of

the cluster along with the α-amino and α-carboxylate groups to form an octahedral coordination sphere (Fig. 1D, Fig. S3B, and Fig. S4B) (44).

Putative Viperin Active Site. Two narrow passageways lead to the [4Fe-4S] cluster bound to viperin. One has a diameter of 6 Å and forms part of the putative active site cavity, as it leads directly to C5′ of SAH and 5′-dAdo, the site of radical formation (Fig. 2A). The second passageway is located on the opposite side of the protein and is formed by Leu264, Arg265, and the cluster-binding loop (Fig. S5). The active site cavity is formed by residues from strands β_1-β_6 and the beginning of the C-terminal extension. These residues line the β-barrel with their side chains directed towards its interior (Fig. 2B). The active site residues supply five positively charged (Lys120, Lys220, Arg245, Lys247, and Lys297), one negatively charged (Glu293), ten additional hydrophilic, and seven hydrophobic side chains (Fig. 2B).

Viperin Crystal Packing Interactions. The asymmetric unit of viperin crystals contains two molecules that interact through several salt bridges that are formed between the positively charged active site residues of one molecule and negatively charged residues in the loop following β_6 of a second molecule (Fig. S6). This head-to-tail interaction, together with the crystallographic twofold screw axis, generates pseudo-fourfold screw axis symmetry along the **c** axis of the unit cell. The interface between the two viperin molecules in the asymmetric unit is relatively small (approximately 1000 $Å^2$) (46), lacks twofold symmetry, and hence is not predicted to result in a dimer in solution. However, it is possible that the head-to-tail interactions observed in the crystal contribute to higher order structures or polymerization when viperin is localized at the ER membrane at high concentrations (34).

Sequence Alignments with *M. musculus* Viperin. Viperin is highly conserved within vertebrates although significant sequence variation occurs in the N-terminal region that precedes the β-barrel (8, 47). BLAST searches starting with *M. musculus* viperin show that viperin is highly conserved among 171 vertebrates with sequence identities ranging from roughly 65 to 95%. In addition, the proposed active site residues are conserved. BLAST searches also showed a group of closely related fungal enzymes. Sequence alignments show that both the predicted structures and the putative active sites of the fungal viperin-like proteins are conserved compared to viperin. The fungal enzymes lack the N-terminal extension found in viperin but have a C-terminal extension that shows conservation within the fungal enzymes but is distinct from the viperin C-terminal extension, which itself is highly conserved. While the biological role of the fungal viperin-like enzymes is unknown, it can be safely concluded that viperin and the fungal viperin-like enzymes have the same substrates and/or catalyze the same radical SAM chemistry. BLAST searches also yielded many bacterial and archaebacterial enzymes with low sequence identity (20-40%). With the exception of MoaA, which is found in both prokaryotes and eukaryotes, these enzymes are best characterized as radical SAM enzymes of unknown function.

Comparison of Viperin and MoaA Structures. A DALI search beginning with viperin shows structural similarity to many radical SAM enzymes (Z-scores ranging from 11 to 20) (48). The most similar structures are the anaerobic sulfatase maturating enzyme anSME from *Clostridium perfrigens* (Z-score 19.9) (41), the molybdenum cofactor biosynthetic enzyme MoaA from *Staphylococcus aureus* (49) (Z-score 18.7), the pyruvate formate-lyase activating enzyme PflA from *E. coli* (Z-score 18.1) (50), and the dual specificity RNA methylase RlmN from *E. coli* (Z-score 17.8) (38, 51). Local sequence alignments of viperin to sequences in the Protein Data Bank (PDB) using BLAST show that *S. aureus* MoaA is the only protein that gives

an Expect value less than 10 ($E = 4 \times 10^{-6}$) (52). Furthermore, more than half of ~7,500 sequences (having Expect values < 10) produced from alignments of viperin to the non-redundant protein sequence database using BLAST are predicted to be MoaA.

The results described above led us to examine the similarity between viperin and MoaA (PDB ID 2FB3) in greater detail. MoaA is widely distributed in both prokaryotes and eukaryotes where it uses radical chemistry to catalyze the cyclization of GTP to 3′,8-cylic-GTP in the first step of molybdenum cofactor biosynthesis (53, 54). Superposition of viperin and MoaA shows similar partial $(\beta\alpha)_6$-barrel cores (Fig. 3A). In addition, MoaA has a short N-terminal extension and, like viperin, its C-terminal extension folds over the partial β-barrel and forms a β-hairpin, a loop, and a helical region (49). However, the C-terminal extension of MoaA ligates a second [4Fe-4S] substrate-binding cluster that is not found in viperin. GTP binds to the additional [4Fe-4S] cluster through N1 and the 2-amino group of the guanine base.

The superposition of viperin and MoaA results in clashes between the ribose and guanine moieties of GTP and the C-terminal extension of viperin; however, the structures align remarkably well near the triphosphate-binding site of GTP (Fig. 3B). Similar modified β-barrels are used by both enzymes to form active site channels lined with several positively charged and other hydrophilic residues (Fig. S7). These residues include Arg17, Lys69, Arg71, Thr102, Asn124, Lys163, Asn165, and Arg192 in MoaA and Lys120, Lys220, Lys247, Arg245, Ser75, Asn77, Asn122, Ser154, and Asn222 in viperin. Moreover, the second β-strand and the following SAM binding motif of MoaA (K_{69}IRITGGEPL) are very similar to those of viperin (K_{120}INFSGGEPF), and six active site residues in MoaA (Lys69, Lys163, Arg192, Thr73, Asn165, and Ile194) are similar or identical to and occupy the same locations as active site residues in viperin (Lys120, Lys220, Lys247, Ser124, Asn222, and Phe249, respectively). The

structural comparison shows that viperin likely contains a triphosphate binding site and, while viperin and MoaA almost certainly catalyze different chemical reactions, the viperin substrate is probably some form of nucleoside triphosphate.

Comparison of Viperin and RlmN Structures. Viperin was recently shown to co-precipitate with dengue virus type-2 RNA (17). RlmN is a radical SAM enzyme that methylates adenosine 2503 of 23S rRNA and adenosine 37 of a subset of tRNAs and is the only radical SAM RNA-modifying enzyme for which a structure has been reported (38, 51, 55-57) (Fig. S8A). RlmN contains a partial $(\beta\alpha)_6$-barrel core, which superimposes well with that of viperin (DALI Z-score 17.6, DALI rmsd 2.6 Å), and an N-terminal domain for RNA recognition (Fig. S8B). Nucleotides 36-39 of tRNA insert into the active site of RlmN to position A37 for methylation. RlmN binds the 5′-phosphate groups of nucleotides 37-39 via Arg114, Thr116, Asn172, Arg207, Asn307, and Arg344. These residues are similar in type to the residues that bind the triphosphate moiety of GTP in MoaA; however, the architecture is significantly different. Superposition of RlmN/tRNA onto viperin shows numerous clashes between viperin active site side chains and the tRNA loop (Fig. S9). While phosphate binding sites are typically formed by positively charged and hydrogen bond donating residues (58), the local active site architecture surrounding the phosphate groups of a nucleoside triphosphate or RNA would, in general, be expected to be different. Thus, our structural comparisons with MoaA and RlmN, although limited, suggest that the active site of viperin better reflects a binding site for a free or chain-terminal nucleotide than an inner nucleotide of RNA.

Comparison of Predicted Radical SAM Enzymes of Unknown Function with Viperin. Interestingly, a large group of bacterial and archaebacterial radical SAM enzymes of unknown function identified from BLAST searches show significant similarity to viperin. In

general, these viperin-like enzymes lack both the N-terminal extension of viperin and the final 15 C-terminal residues, which are conserved in vertebrate viperins. They also lack the second substrate-binding iron-sulfur cluster found in MoaA, and the sequences are in general more similar to viperin than MoaA. Within the active site, 15 mostly charged and hydrophilic residues are conserved compared to viperin (Fig. 4). Sequence alignments further show that these 15 residues are also highly conserved in viperin or viperin-like enzymes found in protists, fungi, and invertebrate and vertebrate animals. In addition, 14 of these residues are conserved in the green alga *Chlamydomonas reinhardtii*. A sequence alignment of viperin with representative enzymes from all kingdoms of life is shown in Fig. S10. The conservation of the active site residues suggests that viperin and this widely distributed group of viperin-like enzymes have the same or similar substrates and/or catalyze the same or similar chemical reactions.

Materials and Methods

Anaerobic Production and Crystallization. Residues 45-362 of *M. musculus* viperin (viperinΔ44), were over-expressed and purified using a variation of the methods used for preparation of radical SAM enzymes involved in thiamin and B_{12} biosynthesis (26, 59). A gene for viperinΔ44 with a cleavable N-terminal hexahistidine tag was synthesized with codon optimization for expression in *E. coli* and cloned into pET-28 via NcoI and XhoI restriction sites to give the following protein product: NH_2-MGSDKIHHHHHHSSGENLYFQG$_{45}$…W$_{362}$-COOH. A second truncated form of viperin lacking the first 46 amino acids, viperinΔ46, was prepared without gene optimization and was over-expressed and purified using similar procedures: MGSSHHHHHHSSGRENLYFQGHMASMTGGQQMGRGSE$_{47}$… W$_{362}$-COOH. *E. coli* NiCo21(DE3) cells (New England Biolabs) that contained plasmid pSuf (60) were transformed with the plasmid carrying the recombinant viperin gene. Starter cultures grown in

15 mL of lysogeny broth supplemented with kanamycin (40 mg/L) and chloramphenicol (34 mg/L) were transferred to shaker flasks containing 1.85 L of minimal medium (1 X minimal medium salts, 40 mg/L kanamycin, 34 mg/L chloramphenicol, 4 g/L dextrose, 2 mM $MgSO_4$, and 0.1 mM $CaCl_2$). The cultures were shaken at 180 rpm and 37 ºC until the OD_{600} reached 0.5-0.55 and then were placed in a 4 ºC cold room for 2.5 h. L-Cys, $Fe(NH_4)_2(SO_4)_2$, and isopropyl β-D-1-thiogalactopyranoside were added to a final concentration of 0.21 mM, 0.065 mM, and 0.2 mM, respectively, and the cultures were shaken at 50 rpm and 15 ºC for 20 h. The cultures were then chilled to 4 ºC, and the *E. coli* were harvested via centrifugation at 6,000 g and 4 ºC for 15 min and flash frozen in liquid nitrogen.

Frozen cell pellets were thawed in a PVC anaerobic chamber (Coy Laboratory Products), resuspended in lysis buffer (100 mM Tris-HCl, 5 mM dithiothreitol (DTT), 0.4 mg/mL lysozyme, and 1.9 kU benzonase, pH 7.6), incubated for 30-60 min on ice, and lysed further via sonication. The lysate was sealed in centrifuge bottles, transferred to a centrifuge outside of the glove box, and spun at 60,000 g and 4 ºC for 20 min. The spun lysate was brought back into the glove box and the supernatant was subjected to immobilized nickel affinity chromatography employing wash (50 mM Tris-HCl, 300 mM NaCl, 20 mM imidazole, 3 mM DTT, pH 7.4) and elution (50 mM Tris-HCl, 300 mM NaCl, 250 mM imidazole, 3mM DTT, pH 7.5) buffers. The eluate was buffer exchanged into hexahistidine tag cleavage buffer (25 mM Tris-HCl, 125 mM NaCl, 3 mM DTT, pH 7.5) using a Bio-Rad Econo-Pac 10DG desalting column and incubated for 8 h with tobacco-etch virus protease. The reaction mixture was subjected to subtractive immobilized nickel affinity chromatography, buffer exchanged into 5 mM 4-(2-hydroxyethyl)-1-piperazineethanesulfonic acid (HEPES) and 25 mM NaCl, pH 7.1, and flash-frozen in liquid nitrogen.

ViperinΔ44 and viperinΔ46 with bound SAH and viperinΔ44 with bound 5′-dAdo and L-Met were crystallized inside the anaerobic chamber at room temperature using the hanging drop vapor diffusion method. Drops were prepared with a 1:1 ratio of protein-to-reservoir solution. The concentration of viperin was approximately 0.2 mM and the concentrations of SAH (solubilized in dimethylsulfoxide), 5′-dAdo, and L-Met were 5 mM, 5 mM, and 10 mM, respectively. Typical reservoir solutions contained 100 mM HEPES, pH 7.0-7.6, and 20-30% (w/v) polyethylene glycol monomethyl ether (PEG MME) 2000; the concentration of PEG MME 2000 was increased 5-15% in the cryoprotectant.

X-ray Data Collection and Processing. Viperin crystals were exposed to X-rays with wavelengths λ = 0.9792 Å, λ = 0.9793 Å, or 1.7384 Å at 100 K at beamline NE-CAT 24-ID-C of the Advanced Photon Source (APS) (Table S1). X-ray diffraction images were recorded for 1 °/s oscillations on a PILATUS 6MF detector positioned 290 mm (λ = 0.9792 Å), 390 mm (λ = 0.9793 Å), or 220 mm (λ = 1.7384 Å) from the crystal. X-ray images were processed using HKL2000 (61).

Structure Determination and Refinement. The crystal structure of viperin with bound SAH was determined using single-wavelength anomalous diffraction phasing based on the four cluster Fe sites located using SHELXD (62). More than 70% of the protein residues were built automatically using the Autosol module of PHENIX (63). Automated structure refinement was performed using PHENIX (64) and accounted for translation, libration, and screw vibrational motion of partitioned chains (65) (Table S2). Manual model building was performed using COOT (66). Structural and electron density illustrations were made using Chimera (67) and PyMOL (68).

Acknowledgements

Y.L. and P.C. acknowledge Dr. Jiashee Hee for valuable discussions and Susan Mitchell for technical assistance.

References

1. O'Neill LA & Bowie AG (2010) Sensing and signaling in antiviral innate immunity. *Curr Biol* 20(7):R328-333.

2. Takeuchi O & Akira S (2010) Pattern recognition receptors and inflammation. *Cell* 140(6):805-820.

3. Isaacs A & Lindenmann J (1957) Virus interference. I. The interferon. *Proc R Soc Lond B Biol Sci* 147(927):258-267.

4. de Veer MJ, *et al.* (2001) Functional classification of interferon-stimulated genes identified using microarrays. *J Leukoc Biol* 69(6):912-920.

5. Der SD, Zhou A, Williams BR, & Silverman RH (1998) Identification of genes differentially regulated by interferon alpha, beta, or gamma using oligonucleotide arrays. *Proc Natl Acad Sci U S A* 95(26):15623-15628.

6. Samuel CE (2001) Antiviral actions of interferons. *Clin Microbiol Rev* 14(4):778-809.

7. Stark GR, Kerr IM, Williams BR, Silverman RH, & Schreiber RD (1998) How cells respond to interferons. *Annu Rev Biochem* 67:227-264.

8. Chin KC & Cresswell P (2001) Viperin (cig5), an IFN-inducible antiviral protein directly induced by human cytomegalovirus. *Proc Natl Acad Sci U S A* 98(26):15125-15130.

9. Zhu H, Cong JP, & Shenk T (1997) Use of differential display analysis to assess the effect of human cytomegalovirus infection on the accumulation of cellular RNAs: induction of interferon-responsive RNAs. *Proc Natl Acad Sci U S A* 94(25):13985-13990.

10. Boudinot P, *et al.* (2000) Vesicular stomatitis virus and pseudorabies virus induce a vig1/cig5 homologue in mouse dendritic cells via different pathways. *J Gen Virol* 81(Pt 11):2675-2682.

11. Olofsson PS, *et al.* (2005) The antiviral cytomegalovirus inducible gene 5/viperin is expressed in atherosclerosis and regulated by proinflammatory agents. *Arterioscler Thromb Vasc Biol* 25(7):e113-116.

12. Severa M, Coccia EM, & Fitzgerald KA (2006) Toll-like receptor-dependent and -independent viperin gene expression and counter-regulation by PRDI-binding factor-1/BLIMP1. *J Biol Chem* 281(36):26188-26195.

13. Nasr N, *et al.* (2012) HIV-1 infection of human macrophages directly induces viperin which inhibits viral production. *Blood* 120(4):778-788.

14. Szretter KJ, *et al.* (2011) The interferon-inducible gene viperin restricts West Nile virus pathogenesis. *J Virol* 85(22):11557-11566.

15. Helbig KJ, *et al.* (2011) The antiviral protein viperin inhibits hepatitis C virus replication via interaction with nonstructural protein 5A. *Hepatology* 54(5):1506-1517.

16. Jiang D, *et al.* (2008) Identification of three interferon-inducible cellular enzymes that inhibit the replication of hepatitis C virus. *J Virol* 82(4):1665-1678.

17. Helbig KJ, *et al.* (2013) Viperin is induced following dengue virus type-2 (DENV-2) infection and has anti-viral actions requiring the C-terminal end of viperin. *PLoS Negl Trop Dis* 7(4):e2178.

18. Wang X, Hinson ER, & Cresswell P (2007) The interferon-inducible protein viperin inhibits influenza virus release by perturbing lipid rafts. *Cell Host Microbe* 2(2):96-105.

19. Upadhyay AS, *et al.* (2014) Viperin is an iron-sulfur protein that inhibits genome synthesis of tick-borne encephalitis virus via radical SAM domain activity. *Cell Microbiol* 16(6):834-848.

20. Fitzgerald KA (2011) The interferon inducible gene: Viperin. *J Interferon Cytokine Res* 31(1):131-135.

21. Sofia HJ, Chen G, Hetzler BG, Reyes-Spindola JF, & Miller NE (2001) Radical SAM, a novel protein superfamily linking unresolved steps in familiar biosynthetic pathways with radical mechanisms: functional characterization using new analysis and information visualization methods. *Nucleic acids research* 29(5):1097-1106.

22. Nicolet Y & Drennan CL (2004) AdoMet radical proteins--from structure to evolution--alignment of divergent protein sequences reveals strong secondary structure element conservation. *Nucleic acids research* 32(13):4015-4025.

23. Berkovitch F, Nicolet Y, Wan JT, Jarrett JT, & Drennan CL (2004) Crystal structure of biotin synthase, an *S*-adenosylmethionine-dependent radical enzyme. *Science* 303(5654):76-79.

24. Broderick JB, Duffus BR, Duschene KS, & Shepard EM (2014) Radical *S*-adenosylmethionine enzymes. *Chem Rev* 114(8):4229-4317.

25. Chatterjee A*, et al.* (2008) Reconstitution of ThiC in thiamine pyrimidine biosynthesis expands the radical SAM superfamily. *Nat Chem Biol* 4(12):758-765.

26. Fenwick MK*, et al.* (2015) Non-canonical active site architecture of the radical SAM thiamin pyrimidine synthase. *Nat Commun* 6:6480.

27. Frey PA, Hegeman AD, & Ruzicka FJ (2008) The Radical SAM Superfamily. *Crit Rev Biochem Mol Biol* 43(1):63-88.

28. Layer G, Moser J, Heinz DW, Jahn D, & Schubert WD (2003) Crystal structure of coproporphyrinogen III oxidase reveals cofactor geometry of Radical SAM enzymes. *EMBO J* 22(23):6214-6224.

29. Lepore BW, Ruzicka FJ, Frey PA, & Ringe D (2005) The x-ray crystal structure of lysine-2,3-aminomutase from *Clostridium subterminale*. *Proc Natl Acad Sci U S A* 102(39):13819-13824.

30. Petrovich RM, Ruzicka FJ, Reed GH, & Frey PA (1992) Characterization of iron-sulfur clusters in lysine 2,3-aminomutase by electron paramagnetic resonance spectroscopy. *Biochemistry* 31(44):10774-10781.

31. Zhang Y*, et al.* (2010) Diphthamide biosynthesis requires an organic radical generated by an iron-sulphur enzyme. *Nature* 465(7300):891-896.

32. Duschene KS & Broderick JB (2010) The antiviral protein viperin is a radical SAM enzyme. *FEBS Lett* 584(6):1263-1267.

33. Hinson ER & Cresswell P (2009) The antiviral protein, viperin, localizes to lipid droplets via its N-terminal amphipathic alpha-helix. *Proc Natl Acad Sci U S A* 106(48):20452-20457.

34. Hinson ER & Cresswell P (2009) The N-terminal amphipathic alpha-helix of viperin mediates localization to the cytosolic face of the endoplasmic reticulum and inhibits protein secretion. *J Biol Chem* 284(7):4705-4712.

35. Dosztanyi Z, Csizmok V, Tompa P, & Simon I (2005) IUPred: web server for the prediction of intrinsically unstructured regions of proteins based on estimated energy content. *Bioinformatics* 21(16):3433-3434.

36. Walsby CJ, Ortillo D, Broderick WE, Broderick JB, & Hoffman BM (2002) An anchoring role for FeS clusters: chelation of the amino acid moiety of *S*-adenosylmethionine to the unique iron site of the [4Fe-4S] cluster of pyruvate formate-lyase activating enzyme. *J Am Chem Soc* 124(38):11270-11271.

37. Vey JL & Drennan CL (2011) Structural insights into radical generation by the radical SAM superfamily. *Chem Rev* 111(4):2487-2506.

38. Boal AK, *et al.* (2011) Structural basis for methyl transfer by a radical SAM enzyme. *Science* 332(6033):1089-1092.

39. Dinis P, *et al.* (2015) X-ray crystallographic and EPR spectroscopic analysis of HydG, a maturase in [FeFe]-hydrogenase H-cluster assembly. *Proc Natl Acad Sci U S A* 112(5):1362-1367.

40. Goldman PJ, Grove TL, Booker SJ, & Drennan CL (2013) X-ray analysis of butirosin biosynthetic enzyme BtrN redefines structural motifs for AdoMet radical chemistry. *Proc Natl Acad Sci U S A* 110(40):15949-15954.

41. Goldman PJ, *et al.* (2013) X-ray structure of an AdoMet radical activase reveals an anaerobic solution for formylglycine posttranslational modification. *Proc Natl Acad Sci U S A* 110(21):8519-8524.

42. McLaughlin MI, *et al.* (2016) Crystallographic snapshots of sulfur insertion by lipoyl synthase. *Proc Natl Acad Sci U S A* 113(34):9446-9450.

43. Nicolet Y, Amara P, Mouesca JM, & Fontecilla-Camps JC (2009) Unexpected electron transfer mechanism upon AdoMet cleavage in radical SAM proteins. *Proc Natl Acad Sci U S A* 106(35):14867-14871.

44. Chen D, Walsby C, Hoffman BM, & Frey PA (2003) Coordination and mechanism of reversible cleavage of *S*-adenosylmethionine by the [4Fe-4S] center in lysine 2,3-aminomutase. *J Am Chem Soc* 125(39):11788-11789.

45. Kampmeier JA (2010) Regioselectivity in the homolytic cleavage of *S*-adenosylmethionine. *Biochemistry* 49(51):10770-10772.

46. Krissinel E & Henrick K (2007) Inference of macromolecular assemblies from crystalline state. *J Mol Biol* 372(3):774-797.

47. Boudinot P, Massin P, Blanco M, Riffault S, & Benmansour A (1999) vig-1, a new fish gene induced by the rhabdovirus glycoprotein, has a virus-induced homologue in humans and shares conserved motifs with the MoaA family. *J Virol* 73(3):1846-1852.

48. Holm L & Rosenstrom P (2010) Dali server: conservation mapping in 3D. *Nucleic acids research* 38(Web Server issue):W545-549.

49. Hanzelmann P & Schindelin H (2006) Binding of 5'-GTP to the C-terminal FeS cluster of the radical *S*-adenosylmethionine enzyme MoaA provides insights into its mechanism. *Proc Natl Acad Sci U S A* 103(18):6829-6834.

50. Vey JL*, et al.* (2008) Structural basis for glycyl radical formation by pyruvate formate-lyase activating enzyme. *Proc Natl Acad Sci U S A* 105(42):16137-16141.

51. Schwalm EL, Grove TL, Booker SJ, & Boal AK (2016) Crystallographic capture of a radical *S*-adenosylmethionine enzyme in the act of modifying tRNA. *Science* 352(6283):309-312.

52. Altschul SF, Gish W, Miller W, Myers EW, & Lipman DJ (1990) Basic local alignment search tool. *J Mol Biol* 215(3):403-410.

53. Hover BM, Tonthat NK, Schumacher MA, & Yokoyama K (2015) Mechanism of pyranopterin ring formation in molybdenum cofactor biosynthesis. *Proc Natl Acad Sci U S A* 112(20):6347-6352.

54. Mehta AP, Abdelwahed SH, & Begley TP (2015) Molybdopterin biosynthesis-Mechanistic studies on a novel MoaA catalyzed insertion of a purine carbon into the ribose of GTP. *Biochim Biophys Acta* 1854(9):1073-1077.

55. Grove TL, *et al.* (2011) A radically different mechanism for *S*-adenosylmethionine-dependent methyltransferases. *Science* 332(6029):604-607.

56. Toh SM, Xiong L, Bae T, & Mankin AS (2008) The methyltransferase YfgB/RlmN is responsible for modification of adenosine 2503 in 23S rRNA. *RNA* 14(1):98-106.

57. Yan F, *et al.* (2010) RlmN and Cfr are radical SAM enzymes involved in methylation of ribosomal RNA. *J Am Chem Soc* 132(11):3953-3964.

58. Copley RR & Barton GJ (1994) A structural analysis of phosphate and sulphate binding sites in proteins. Estimation of propensities for binding and conservation of phosphate binding sites. *J Mol Biol* 242(4):321-329.

59. Mehta AP, *et al.* (2015) Anaerobic 5-hydroxybenzimidazole formation from aminoimidazole ribotide: an unanticipated intersection of thiamin and vitamin B12 biosynthesis. *J Am Chem Soc* 137(33):10444-10447.

60. Hanzelmann P, *et al.* (2004) Characterization of MOCS1A, an oxygen-sensitive iron-sulfur protein involved in human molybdenum cofactor biosynthesis. *J Biol Chem* 279(33):34721-34732.

61. Otwinoski Z & Minor W (1997) Processing of X-ray diffraction data collected in oscillation mode. *Method Enzymol* 276:307-326.

62. Schneider TR & Sheldrick GM (2002) Substructure solution with SHELXD. *Acta Crystallogr* D58:1772-1779.

63. Terwilliger TC, *et al.* (2009) Decision-making in structure solution using Bayesian estimates of map quality: the PHENIX AutoSol wizard. *Acta Crystallogr D Biol Crystallogr* 65(Pt 6):582-601.

64. Adams PD, *et al.* (2011) The Phenix software for automated determination of macromolecular structures. *Methods* 55(1):94-106.

65. Painter J & Merritt EA (2006) Optimal description of a protein structure in terms of multiple groups undergoing TLS motion. *Acta Crystallogr.* D62:439-450.

66. Emsley P, Lohkamp B, Scott WG, & Cowtan K (2010) Features and development of Coot. *Acta Crystallogr* D66:486-501.

67. Pettersen EF, *et al.* (2004) UCSF Chimera--a visualization system for exploratory research and analysis. *J Comput Chem* 25(13):1605-1612.

68. DeLano WL (2002) The PyMOL Molecular Graphics System (DeLano Scientific, San Carlos, CA).

69. Dolinsky TJ, Nielsen JE, McCammon JA, & Baker NA (2004) PDB2PQR: an automated pipeline for the setup of Poisson-Boltzmann electrostatics calculations. *Nucleic acids research* 32(Web Server issue):W665-667.

70. Baker NA, Sept D, Joseph S, Holst MJ, & McCammon JA (2001) Electrostatics of nanosystems: application to microtubules and the ribosome. *Proc Natl Acad Sci U S A* 98(18):10037-10041.

Figure Legends

Fig. 1. Overall structure of viperin. (A) Ribbon diagram of viperin with SAH shown as balls and sticks, the [4Fe-4S] cluster shown as brown and yellow spheres, and the three cysteine residues of the [4Fe-4S] cluster-binding motif shown as sticks. The partial $(\beta\alpha)_6$-barrel fold, N-terminal extension, and C-terminal extension are colored light blue, salmon, and light green, respectively. (B) Topology diagram for viperin. β-strands and helices are represented by thick arrows and cylinders, respectively. AH1 denotes the excised putative membrane-associating amphipathic helix. (C) Stereoview of SAH binding site. (D) Stereoview of 5′-dAdo and L-Met binding sites. Potential hydrogen bonds are shown as dashed lines and water molecules are shown as red spheres.

Fig. 2. Structure of the viperin active site cavity. (A) Surface representation of viperin showing a narrow passageway leading to C5′ of SAH, the predicted site of radical formation. (B) Stereoview of the active site cavity. Residues in the partial $(\beta\alpha)_6$-barrel fold, N-terminal extension, and C-terminal extension are colored light blue, salmon, and light green, respectively.

Fig 3. Structural comparison of viperin and *S. aureus* MoaA. (A) Superimposition of MoaA onto viperin. The partial $(\beta\alpha)_6$-barrel fold, N-terminal extension, and C-terminal extension of viperin are colored light blue, salmon, and light green, respectively. The corresponding regions of MoaA are colored goldenrod, dark red, and navy blue. SAH bound to viperin is shown as balls and sticks. GTP bound to MoaA is not shown for clarity. The [4Fe-4S] clusters and the cysteine residues that ligate the irons are shown as sticks. (B) Active site comparison of viperin and MoaA. GTP bound to MoaA is shown as balls and sticks. The side chains of 22 active site residues of viperin and the side chains of eight residues of MoaA that reside within 4 Å of the phosphate groups of GTP are shown.

Fig. 4. Stereoview of viperin active site showing conserved residues found in viperin or viperin-like enzymes from all kingdoms of life. Viperin-like enzymes were identified by searching for the active site residues of *M. musculus* viperin in a large set of sequences aligned to *M. musculus* viperin using BLAST with an Expect value of 10. Fifteen active site residues (represented with magenta sticks) were found to be conserved.

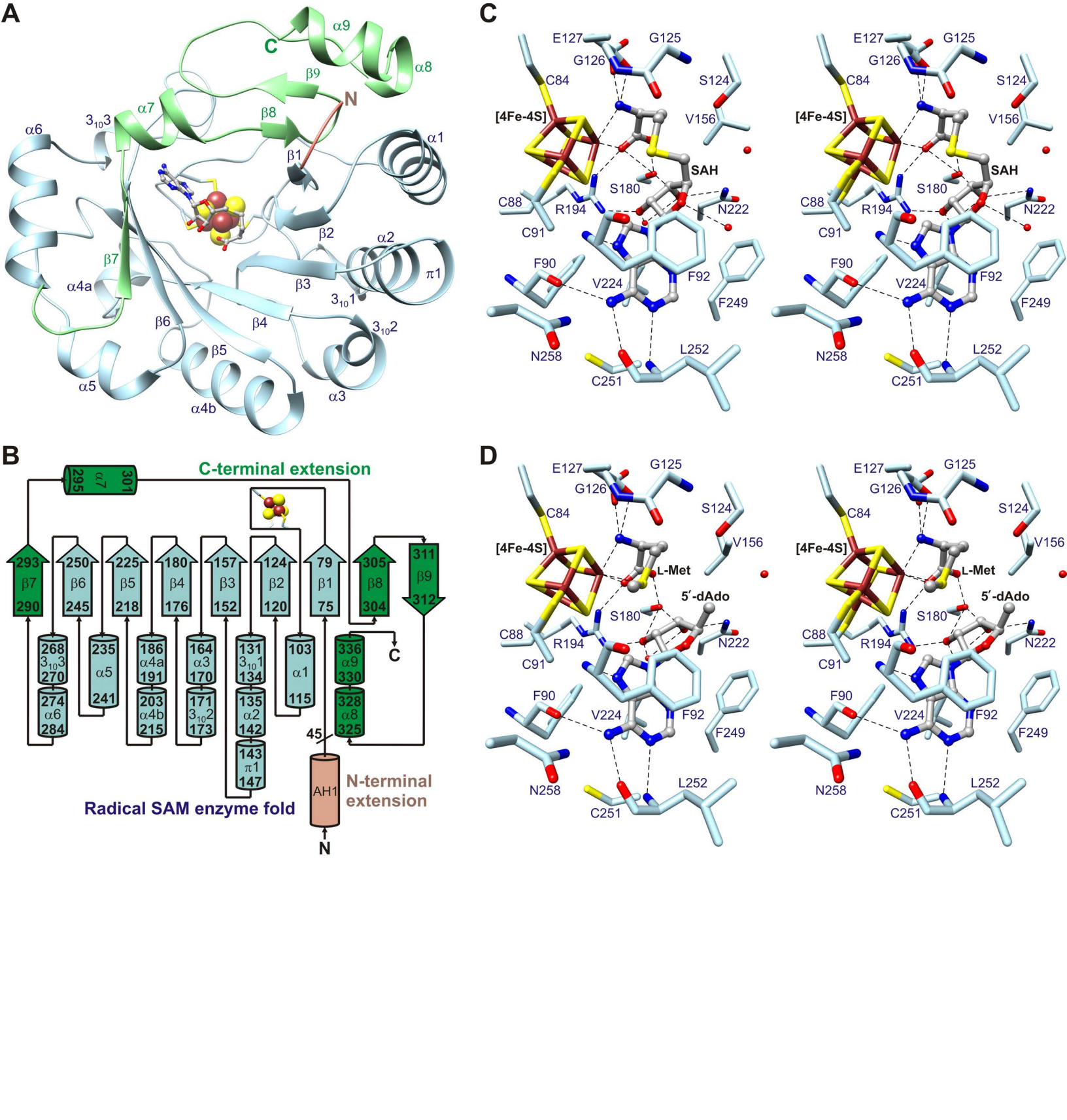
A
C
α9
α8
β9
N
α7
β8
α6
3103
α1
β1
β2
α2
β7
α4a
β3
π1
3101
β6
β4
3102
β5
α5
α4b
α3
B
C-terminal extension
295
α7
301
293
β7
290
250
β6
245
225
β5
218
180
β4
176
157
β3
152
124
β2
120
79
β1
75
305
β8
304
311
β9
312
268
3103
270
274
α6
284
235
α5
241
186
α4a
191
203
α4b
215
164
α3
170
171
3102
173
131
3101
134
135
α2
142
143
π1
147
103
α1
115
336
α9
330
328
α8
325
C
45
AH1
N
Radical SAM enzyme fold
N-terminal
extension
C
E127
G125
G126
C84
S124
[4Fe-4S]
V156
SAH
S180
C88
R194
N222
C91
F90
V224
F92
F249
N258
L252
C251
D
L-Met
5′-dAdo

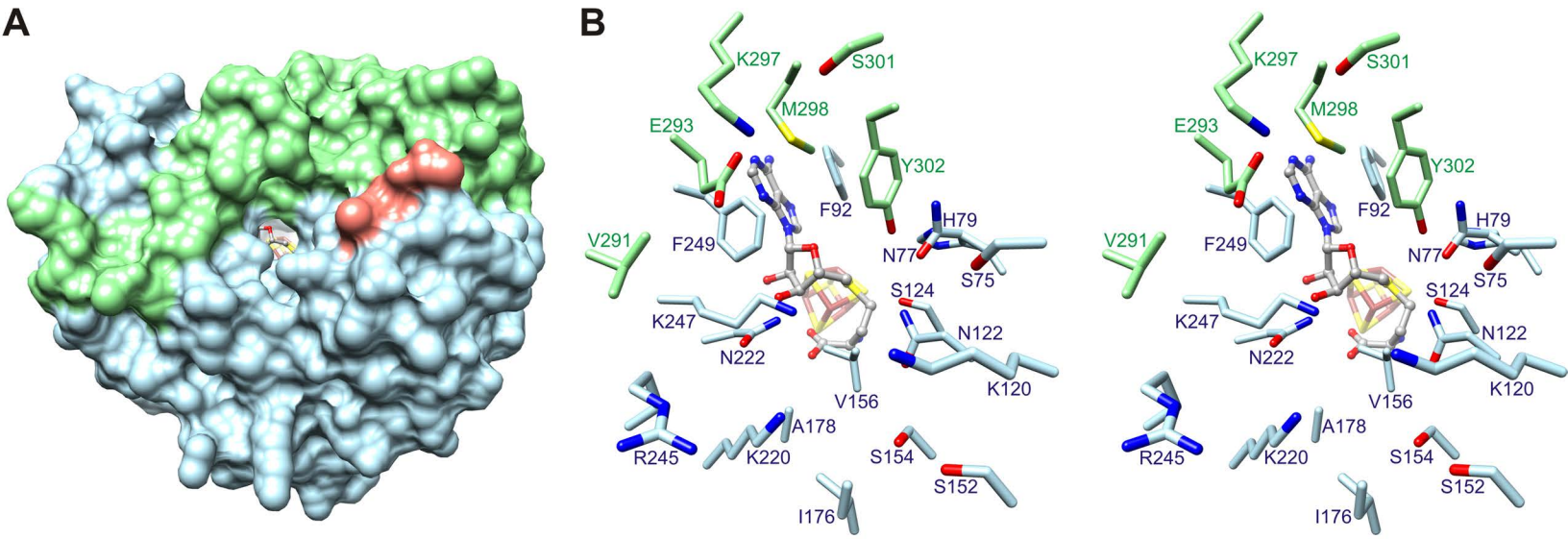
A
B
K297
S301
M298
E293
Y302
F92
H79
V291
F249
N77
S75
S124
K247
N122
N222
K120
V156
A178
R245
K220
S154
S152
I176

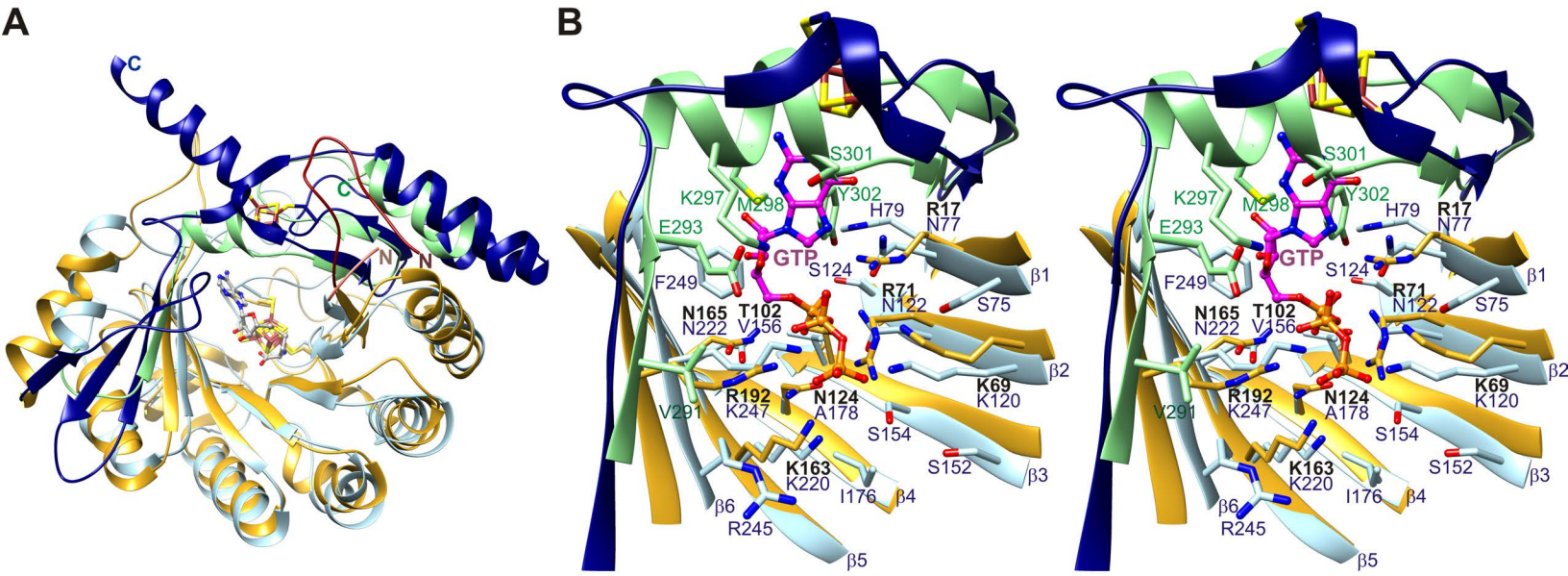
A
C
C
N
N
B
S301
K297
M298
Y302
H79
R17
N77
E293
GTP
S124
F249
R71
N122
S75
β1
N165
N222
T102
V156
β2
K69
K120
R192
K247
N124
A178
V291
S154
S152
β3
K163
K220
I176
β4
β6
R245
β5

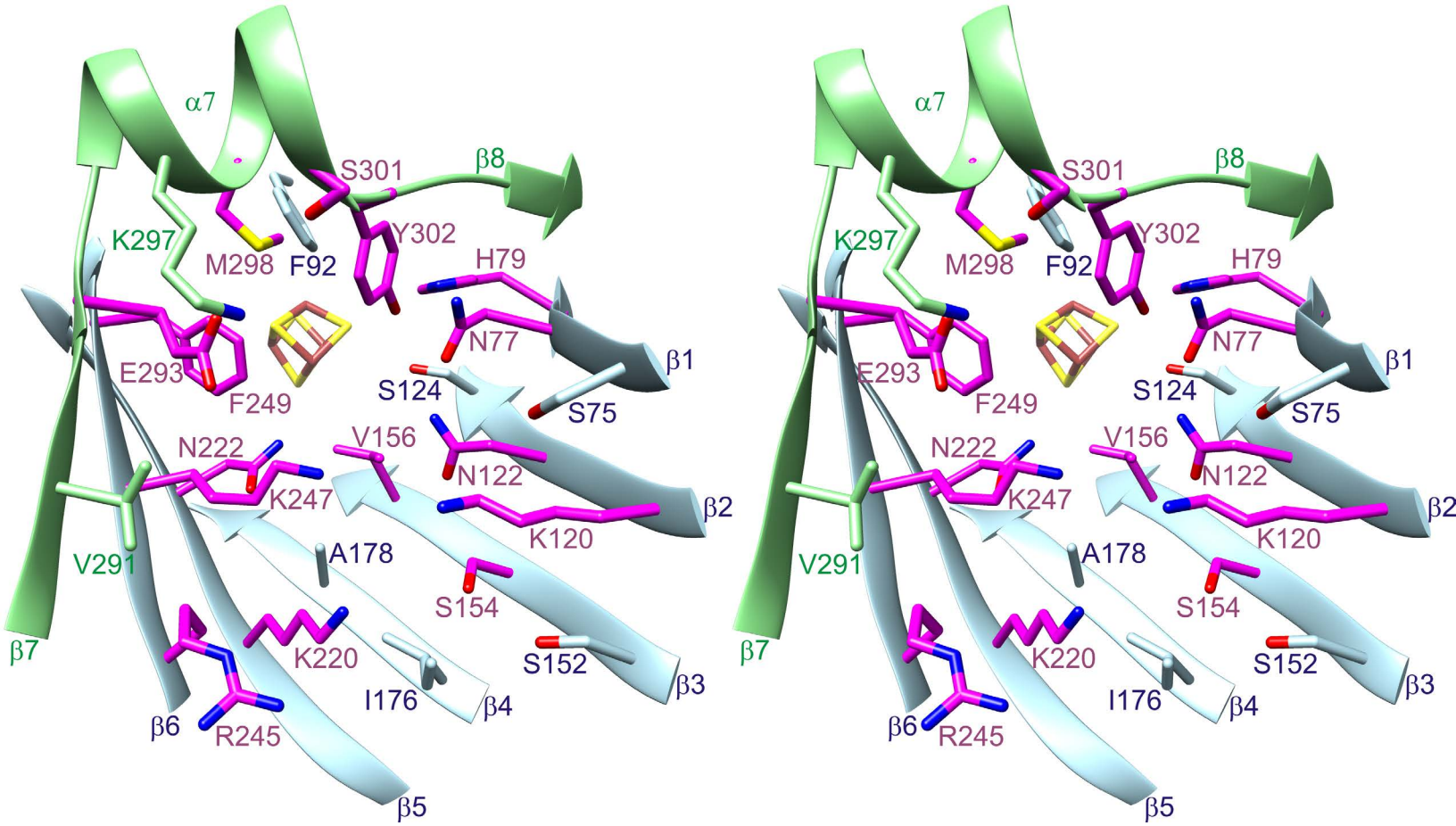
α7
S301
β8
K297
M298
F92
Y302
H79
N77
β1
E293
F249
S124
S75
N222
V156
N122
K247
β2
K120
V291
A178
S154
β7
K220
S152
β3
I176
β4
β6
R245
β5
α7
S301
β8
K297
M298
F92
Y302
H79
N77
β1
E293
F249
S124
S75
N222
V156
N122
K247
β2
K120
V291
A178
S154
β7
K220
S152
β3
I176
β4
β6
R245
β5